Journal of Materials Chemistry A

Mesoporous Carbon Cubes Derived from Fullerene Crystals as a High Rate Performance Electrode Material for Supercapacitors

Journal:	*Journal of Materials Chemistry A*
Manuscript ID	TA-ART-01-2019-000520.R1
Article Type:	Paper
Date Submitted by the Author:	18-Apr-2019
Complete List of Authors:	Bairi, Partha; IACS, PSU; National Institute For Materials Science, International Center for Materials Nanoarchitectonics Maji, Subrata; National Institute for Materials Science (NIMS), WPI Center for Materials Nanoarchitectonics (MANA) Hill, Jonathan; National Institute for Materials Science, International Center for Materials Nanoarchitectonics Kim, Jung Ho; Institute for Superconducting and Electronic Materials, Ariga, Katsuhiko; National Institute for Materials Science, World Premier International (WPI) Research Center for Materials Nanoarchitectonics (MANA) Shrestha, Lok Kumar; National Institute for Materials Science (NIMS), WPI Center for Materials Nanoarchitectonics (MANA)

Journal Name

ARTICLE

Mesoporous Carbon Cubes Derived from Fullerene Crystals as a High Rate Performance Electrode Material for Supercapacitors

Received 00th January 20xx,
Accepted 00th January 20xx

DOI: 10.1039/x0xx00000x

www.rsc.org/

Partha Bairi,[a] Subrata Maji,[a] Jonathan P. Hill,[a] Jung Ho Kim,[b] Katsuhiko Ariga [a,c] and Lok Kumar Shrestha[a]*

We report the thermal conversion of three-dimensional (3D) mesoporous crystalline fullerene C_{70} cubes (MCFC) into mesoporous carbon with retention of the original cubic morphology. This newly synthesized cube morphology mesoporous carbon shows excellent electrochemical capacitive properties. Cyclic voltammetry and chronopotentiometry (charge–discharge) measurements reveal that this nanostructured carbon material exhibits very high specific capacitance *ca.* 286 F g^{-1} at a scan rate of 5 mV s^{-1} and 205 F g^{-1} at a current density of 1 A g^{-1}. Furthermore, it exhibits high rate performance and excellent cyclic stability, no loss of specific capacitance is observed after 10,000 cycles. We believe that this novel mesoporous cubic carbon can be used as an excellent electrode material for advanced electrochemical supercapacitors.

Introduction

Electrochemical capacitors or supercapacitors are considered to be effective and eco-friendly energy storage devices.[1-5] Supercapacitors are currently used in memory backup systems, consumer electronic devices, and industrial power and energy management systems. Their excellent utility is illustrated by their use in state-of-the-art aerospace applications, for instance, in the Airbus A380.[2] The main disadvantage of supercapacitors is their low energy density (1-10 $Whkg^{-1}$) compared to lead acid batteries (30-40 $Whkg^{-1}$), lithium ion batteries (10-250 $Whkg^{-1}$) and fuel cells.[6] Therefore, current supercapacitor research is focused on the increasing their energy densities to improve competitiveness with battery-based devices. The energy density of supercapacitors can be improved either by improving the specific capacitance (*C*) of the active electrode materials or by widening the operation voltage (*V*) window since energy stored is proportional to CV^2.[1-6] Widening the potential window of the cell has been achieved by using ionic liquids.[6] However, ionic liquids are limited by their low ionic conductivities, large cost and air sensitivity so that improving the specific capacitance of the active electrode materials is a better means of enhancing the energy density of supercapacitors. Mesoporous carbons are the leading electrode materials for commercial supercapacitors considering their outstanding cycle stability, good rate capability, wide-ranging operating voltage, high abundance and low cost.[7] This is despite the very low specific capacitance of conventional mesoporous carbon. Therefore, the preparation of novel mesoporous carbons with very high specific capacitances is required. Extensive research has been carried out to develop high-quality carbons having very high surface areas, controllable pore volumes and uniform pore size distributions. Hard and soft templating methods are well known as being powerful tools for the production of high quality mesoporous carbons.[8-14] However, reports of the morphology controlled synthesis of very high surface area mesoporous carbon remain limited. The morphology of carbon materials plays a critical role in supercapacitor device operation with 1D-type materials being suitable for optimizing charge/ion transport whereas 2D-type materials are more appropriate for making flexible supercapacitor devices. 3D-type materials, on the other hand, provide a large area electrolyte–electrode interface and continuous electron transport path.[15,16]

Fullerene (here C_{70}), which can be regarded as a zero-dimensional functional molecule, forms higher dimensionality crystalline nanostructures at interfaces.[17-20] Self-assembled fullerene nanostructures can be converted directly into nanoporous carbon with retention of the original morphology of the starting fullerene nanostructure.[21-23] Mesoporous framework carbon derived from fullerenes are expected to display excellent capacitive properties because of their well-defined and robust structures.[21-23]

Here we report direct conversion of mesoporous crystalline fullerene C_{70} cubes (MCFC) into mesoporous carbon which possesses a high specific surface area and retains the cubic morphology of MCFC even after heating at 900 °C (MCFC-900). MCFC was produced at a liquid-liquid interface followed by mild thermal activation (Scheme 1). Our newly synthesized mesoporous carbon cubes exhibit very high specific

[a] *International Center for Materials Nanoarchitectonics (WPI-MANA), National Institute for Materials Science (NIMS), 1-1 Namiki, Tsukuba 305-0044, Japan*
[b] *Institute for Superconducting and Electronic Materials (ISEM), Australian Institute for Innovative Materials (AIIM), University of Wollongong, North Wollongong, NSW 2500, Australia*
[c] *Department of Advanced Materials Science, Graduate School of Frontier Sciences, The University of Tokyo, 5-1-5 Kashiwanoha, Kashiwa, Chiba 277-8561, Japan*
*Corresponding authors: *SHRESTHA.Lokkumar@nims.go.jp*
†Electronic Supplementary Information (ESI) available: Additional SEM, TEM, HR-TEM, FT-IR, TGA, XPS and CV data. See DOI: 10.1039/x0xx00000x

capacitances compared to carbon nanotube, graphene and commercial activated carbons with values at ca. 286 F g^{-1} at a scan rate of 5 mV s^{-1} and 205 F g^{-1} at a current density of 1 A g^{-1}. Excellent retention of specific capacitance was observed at high current density and fast scan rates indicating a high rate performance for MCFC-900. It also exhibits excellent cyclic stability with no loss of specific capacitance observed even after 10,000 cycles.

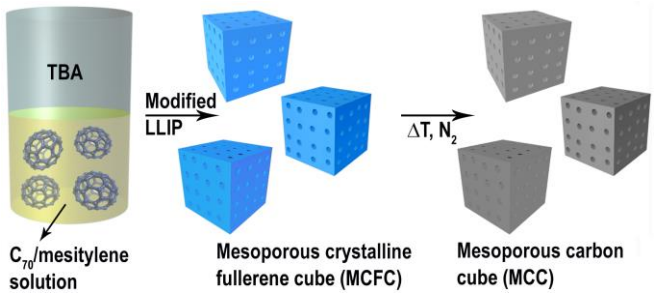

Scheme 1. Schematic Representation of the Fabrication of MCFC at a Liquid-Liquid Interface and their Direct Conversion into Mesoporous Carbon Cubes upon Heat-Treatment at High Temperatures

Experimental section

Synthesis of MCFC, MCFC-900 and MCFC-2000

MCFC was synthesized using a liquid-liquid interfacial precipitation (LLIP) method followed by mild heat treatment.[24] Mesitylene and *tert*-butyl alcohol (TBA) were used respectively as solvent and anti-solvent for C_{70} (99 % pure, MTR Ltd., USA) in the LLIP process. An interface was prepared by slowly adding TBA (5 mL) to a solution of C_{70} in mesitylene (1 mL, c = 1 mg mL^{-1}) at 25 °C. The resulting reaction mixture was stored without agitation in an incubator for 3 h. The reaction mixture was then sonicated for 30 s followed by gentle manual agitation (shaking of the vial). The mixed solution was then stored in an incubator for 2 days at 25 °C. The reaction mixture was then stirred for 3 days at 75 °C and separated by centrifugation. The obtained solid was dried at 80 °C under reduced pressure for 24 h and the product is referred to as mesoporous crystalline fullerene C_{70} cubes (MCFC).[9] MCFC-900 was prepared by heating dry MCFC at 900 °C under the nitrogen atmosphere. Heating to 900 °C was at a heating rate of 2 °C min^{-1} with the temperature subsequently maintained at 900 °C for 2 h. The temperature was returned to ambient at a cooling rate of 10 °C min^{-1}. Dry MCFC powder was heat-treated at 2000 °C in a vacuum (7 × 10^{-3} Pa) using an FVHP-1-3, FTR-20-3VH (Fujidempa Kogyo Co., Ltd, Osaka, Japan) to obtain MCFC-2000.

Characterizations

Scanning electron microscopy (SEM) images of MCFC, MCFC-900 and MCFC-2000 were obtained using a Hitachi Model S-4800 field effect scanning electron microscope (FE-SEM) operating at an accelerating voltage of 10 kV. To prevent charging, all samples were coated with platinum (~ 2 nm) by sputtering using a Hitachi S-2030 ion coater. Transmission electron microscopy (TEM) images and selected area electron diffraction patterns (SAED) of MCFC, MCFC-900 and MCFC-2000 were obtained using a transmission electron microscope (JEOL Model JEM-2100F operated at 200 kV). FT-IR spectra of the prepared samples were recorded using a Nicolet 4700 FT-IR instrument, ThermoElectron Corporation. Thermogravimetric analysis (TGA) of MCFC was performed under an argon gas atmosphere at a heating rate of 10 °C min^{-1} using an SII Instrument (Model Exstar 600). Powder X-ray diffraction (pXRD) patterns of pristine C_{70} and all carbon samples were recorded at 25 °C on a Rigaku RINT2000 diffractometer with Cu-Kα radiation (λ = 0.1541 nm). Raman scattering spectra of the carbon samples were measured using a Jobin-Yvon T64000 Raman spectrometer with a green laser of wavelength 514.5 nm at 0.01 mW power. Nitrogen gas adsorption-desorption isotherms of the porous carbon samples were measured on an automatic adsorption instrument (Quantachrome Instruments, Autosorb-iQ2, USA) at liquid nitrogen temperature 77.35 K. X-ray photoelectron spectroscopy (XPS) of all the porous cubic shaped carbon materials and pristine C_{70} was performed on a Theta Probe spectrometer (Thermo Electron Co. Germany) using monochromatic Al-Kα radiation (photon energy 15 KeV, maximum energy resolution 0.47 eV, and maximum space resolution 15 mm). High-resolution spectra for core level C 1s and O 1s were recorded in 0.05 eV steps. To avoid sample charging a built-in electronic charge neutralizing electron flood gun was used.

Electrochemical measurements

Electrochemical performances of MCFC and MCFC-900, MCFC-1500 and MCFC-2000 were studied by cyclic voltammetry (CV) and charge-discharge experiments with a three-electrode system at room temperature. Aqueous 1 M H_2SO_4 solution was used as an electrolyte. For CV and charge-discharge experiments, glassy carbon electrodes were modified with the carbon samples. First, the porous carbon sample was dispersed in a water-ethanol (4:1) mixture with sonication. The GC electrode was modified by drop-casting the dispersed materials onto the GC surface followed by drying at 60 °C. Nafion (0.5 % in ethanol) was used as a binder. All experiments were carried out using an ALS/CH Model 850D Electrochemical Analyzer in the potential range from 0 to 0.8 V (vs. Ag/AgCl). Electrochemical impedance spectroscopy (EIS) measurements were carried out using a CHI 660D electrochemical workstation. EIS measurements were performed at an open-circuit potential within the frequency range of 10-2-105 Hz at amplitude of 5 mV.

Calculations

Capacitance (C_s) was calculated from the galvanostatic discharge process according to the following equation:

$$C_s = \frac{I \times t}{m \times \Delta V} \quad \text{..... (1)}$$

where ΔV is the voltage change (V) during the discharge process, m is the total mass of the active material, I is the discharge current (A) and t is the discharge time (s).

The capacitance of the electrode was calculated from CV according to the following equation:

$$C_s = \frac{\int I dV}{mS\Delta V} \quad \text{..... (2)}$$

where m is the total mass of the active material (g), ΔV is the absolute value of the potential window (V), S is the scan rate (mVs^{-1}), and I is the current (A).

Results and discussion

MCFC was synthesized using the liquid-liquid interfacial precipitation method followed by mild heat treatment.[24] MCFC-900 was prepared by carbonization of MCFC at 900 °C under the nitrogen gas atmosphere. We have also prepared graphitized MCFC at 2000 °C under the reduced pressure with the product obtained being designated MCFC-2000. SEM and TEM analysis (Fig. S1 and S2) indicate that MCFC is a highly crystalline mesoporous cubic crystal with a very narrow size distribution. Average edge size and pore diameter of MCFC are ca. 800 nm and ca. 24 nm, respectively.[24] Pore walls of MCFC are also crystalline in nature as confirmed by HR-TEM and the corresponding selected area diffraction pattern (Fig. S2e). FT-IR and thermogravimetric analyses of MCFC (Fig. S3) indicate that C_{70} forms a solvated structure with mesitylene in MCFC. After heat treatment of MCFC at 900 °C, the cubic morphology of MCFC is retained. SEM images of MCFC-900 (Fig. 1a and S4) show the well-defined 3D cubic morphology and the high porosity structure. The well-developed mesoporous structure can also be seen in TEM (Fig. 1b-e and S5), while HR-TEM (Fig. 1d and S6) images of MCFC-900 show amorphous carbon structure. Treatment of MCFC at 2000 °C, largely destroys the cubic morphology with only a few cubic items remaining in samples (Fig. S7 and S8). HR-TEM images of MCFC-2000 clearly reveal the highly dense graphitic structure with a maximum of nine graphitic layers with interlayer separation ~ 0.344 nm being observed in HR-TEM (Fig. S10).

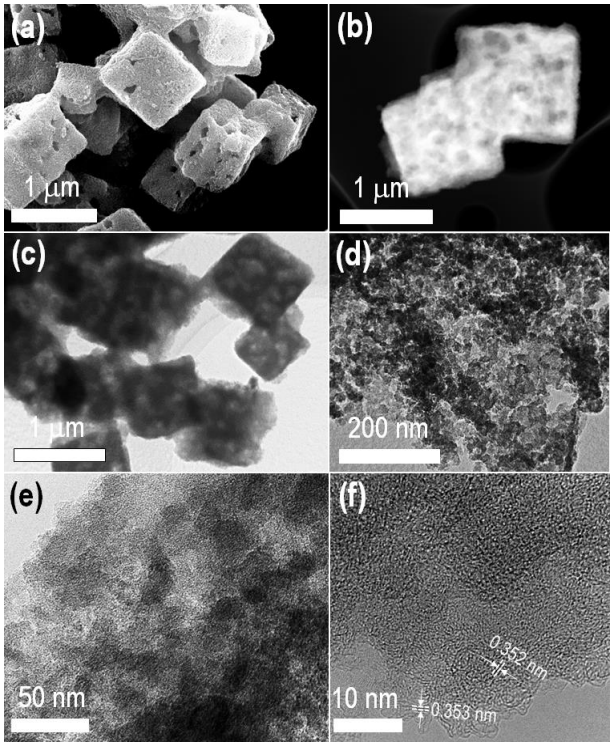

Fig. 1 (a) SEM image of MCFC-900, (b) STEM image of MCFC-900 (c-e) TEM images of MCFC-900 showing the with porous structure and (f) HR-TEM image of MCFC-900.

Nitrogen adsorption-desorption isotherms of MCFC and heat treated MCFC are shown in Fig. 2. The N_2 adsorption–desorption isotherm of MCFC does not exhibit saturation at higher pressures due to the development of larger size pores (Fig. 2a).

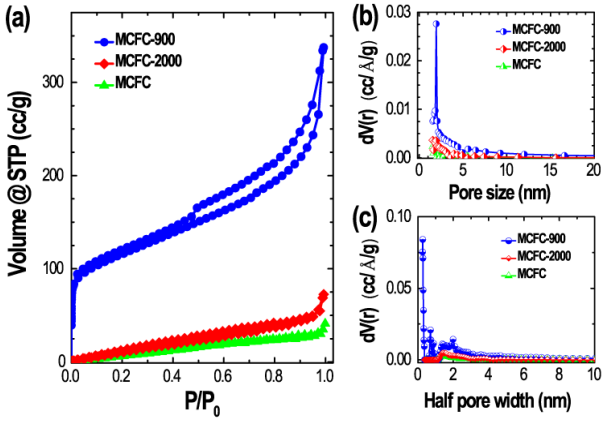

Fig. 2 (a) Nitrogen adsorption–desorption isotherms, (b) Pore size distribution obtained from BJH method and (c) Pore size distribution obtained from NL-DFT method for MCFC, MCFC-900 and MCFC-2000.

The isotherm of mesoporous MCFC-900 has a typical type-IV curve with hysteresis loop indicating a cage-like structure (Fig. 2a). The Brunauer-Emmett-Teller (BET) surface area of HMCFC_900 ca. 642.6 m^2g^{-1} is much larger than that of MCFC (ca. 47.7 m^2g^{-1}). Higher temperature graphitization for MCFC-2000 leads to a low surface area ca. 76.1 m^2g^{-1} probably due to the formation of a higher density carboniferous structure (Fig. S10). Pore size distribution curves obtained by the Barrett-Joyner-Halenda (BJH) method using desorption isotherms (Fig. 2b) and non-local density functional theory (NL-DFT) method (Fig. 2c) indicate the existence of both meso- and microporous structures. Pore sizes were estimated using both the adsorption and desorption BJH pore size distribution curves and were ca. 3.50 nm (MCFC), 3.44 nm (MCFC-900), and 3.21 nm (MCFC-2000). The corresponding pore volumes were ca. 0.065 cc/g (MCFC), 0.367 cc/g (MCFC-900), and 0.103 cc/g (MCFC-2000). Pore size distributions obtained from BJH adsorption are supplied in Fig. S11 and porosity properties are supplied in Table S1-S4.

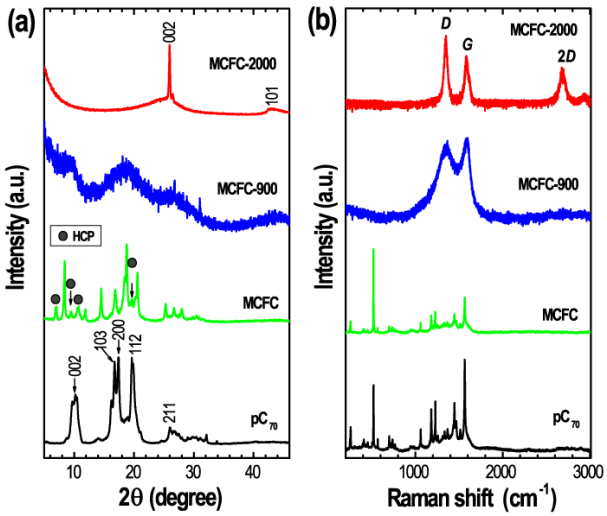

Fig. 3 (a) Powder XRD patterns and (b) Raman scattering spectra of pristine C_{70}, MCFC, MCFC-900 and MCFC-2000.

The structural characterization of MCFC, heat treated MCFC materials and pC_{70} were performed using powder XRD and Raman spectroscopy. The powder XRD pattern of pristine C_{70} (Fig.3a) indicates a hexagonal closed pack (*hcp*) crystal structure with lattice parameters a = 1.08 and c = 1.74 nm.[20,25] In contrast, MCFC exhibits a mixed crystal phase and can be indexed as simple cubic (*sc*) (Fig.3a) with cell dimension a = 1.05 nm mixed with *hcp* with cell dimensions a = 1.09, and c = 1.73 nm.[20] After carbonization at 900 °C, C_{70} is not fully transformed to amorphous carbon and there remain some diffraction peaks due to crystalline C_{70} (Fig.3a) which indicate the strong interactions existing between C_{70} molecules along the growth axis in its crystals.[22] Graphitization of MCFC at 2000 °C, eliminates X-ray scattering peaks due to crystalline C_{70} with a new sharp diffraction peak due to graphitic carbon appearing at 26.02° (d = 0.342 nm), which corresponds to the (002) plane.[21-23] Furthermore, an additional broad low intensity diffraction peak corresponding to the (101) graphite plane appears at approximately 43.5° (Fig.3a) confirming the presence of weak intralayer-ordering of the graphene layers in MCFC-2000.

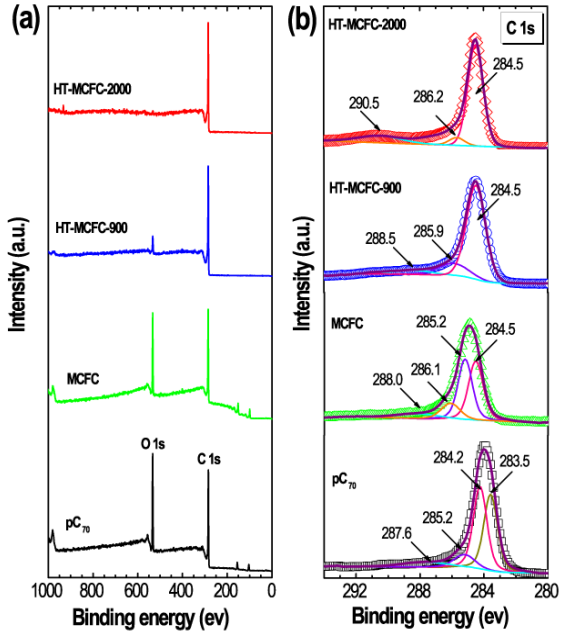

Fig. 4 (a) XPS survey spectra of pC_{70}, MCFC, MCFC-900 and MCFC-2000 and (b) Corresponding C 1s XPS core level spectra with deconvoluted peaks.

Thermal conversion of MCFC into amorphous MCFC-900 and graphitic MCFC-2000 is further confirmed by Raman scattering. The Raman spectrum of MCFC is identical to that of pC_{70} (Fig.3b) suggesting that recrystallization and solvating mesitylene do not affect the rotation of C_{70} molecules.[26] After carbonization, the Raman peaks due to C_{70} are absent with two new peaks appearing in amorphous MCFC-900 at 1350 and 1583 cm^{-1} corresponding to D and G bands (Fig.3b). The D band (defect-induced) indicates the presence of disorder in sp^2 carbon materials while the G band corresponds to the stretching vibration of C–C bond in graphitic structures and is common to all sp^2 carbon systems.[27] In addition to D and G bands, an additional Raman band at 2686 cm^{-1} (2D band) appears in MCFC-2000, and indicates the formation of a highly crystalline carbon material. X-ray photoelectron spectroscopy (XPS) survey spectra of MCFC, MCFC-900, MCFC-2000 and pC_{70} contain C 1s and O 1s core level peaks (Fig. 4a). The presence of oxygen in the prepared samples is due to aerial oxidation. Note that the relative intensities of the O 1s XPS spectra is lower in the heat-treated samples compared to pC_{70} and MCFC prior to heat-treatment. This indicates that aerial oxidation occurs easily in the pristine and self-assembled forms compared to the carbon samples obtained after heat-treatment. The XPS C 1s core level peaks of pC_{70}, MCFC, MCFC_900 and MCFC-2000 (Fig. 4b) reveal that all carbon samples contain oxygenated surface functional groups in addition to the C=C (sp^2), C=C (sp^3) and C=O bonding states of carbon. Corresponding O 1s XPS core level spectra with deconvoluted peaks are also shown in Fig. S12.

To explore potential application in energy storage devices, the electrochemical properties of the MCFC, MCFC-900 and MCFC-2000 materials were investigated by using cyclic voltammetry (CV) and galvanostatic charge–discharge experiments.[28,29] All the electrochemical measurements were recorded in aqueous 1 M H_2SO_4 electrolyte over the potential range 0 to 0.8 V (*vs.* Ag/AgCl) using a three electrode system. In Fig. 5a, we have compared the CV curves of MCFC before and after heat-treatments at a scan rate of 5 mV s^{-1}. Current density of the MCFC-900 modified electrode is much higher than for the MCFC and MCFC-2000, which indicate that MCFC-900 could store higher energy compared to the MCFC and MCFC-2000 samples. The CV curve of MCFC-900 at different scan rates is presented in Fig. 5b.

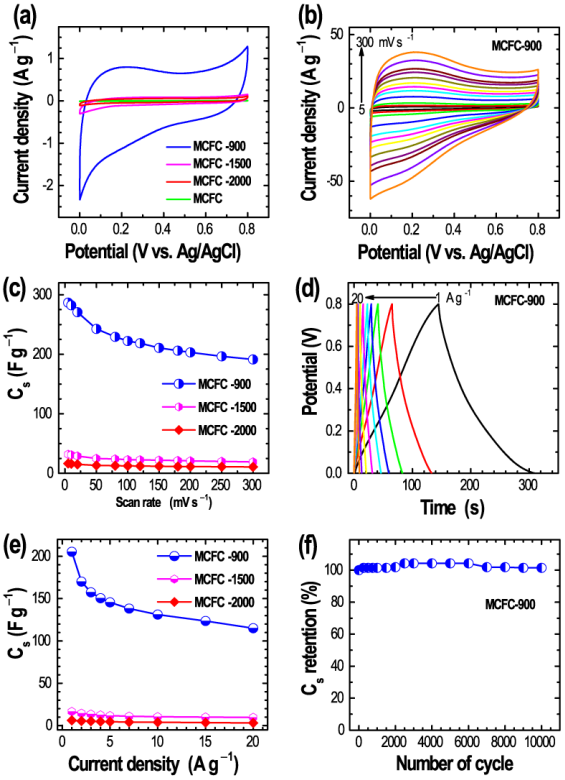

Fig. 5 (a) Comparison of the CV profiles of the all carbon samples at a scan rate of 5 mV s^{-1}, (b) CV curves of mesoporous carbon MCFC-900 at different scan rates (5 to 300 mV s^{-1}), (c) Specific capacitances obtained from CV curves of the MCFC-900, MCFC-1500 and MCFC-2000 at different scan rates, (d) Charge–discharge curves for MCFC-900 at different current densities, (e) Specific capacitance obtained from charge–discharge curves of MCFC-900, MCFC-1500 and MCFC-2000 at different current densities (1 – 20 A g^{-1}), and (f) Cyclic stability of the MCFC-900 modified electrode at 7 A g^{-1}.

It reveals a very rapid current response and exhibits a quasi-rectangular shape at low scan rates, features that are a characteristic of electrical double layer capacitors (EDLCs).[29-34] With increasing scan rates the CV profile departs from a rectangular shape due both to the presence of oxygen-containing surface functional groups and to the obstruction of diffusion of electrolyte ions at mesoporous cube surfaces. Fig. 5c shows specific capacitance vs scan rates for MCFC-900 and MCFC-2000 as typical examples. As it can be seen, MCFC-900 exhibits a large specific capacitance of ca. 286 F g^{-1} at a scan rate 5 mV s^{-1} compared to MCFC-2000 sample, which exhibits specific capacitance of ca. 16 F g^{-1} (at 5 mV s^{-1}). The large specific capacitance of MCFC-900 is sustained even at very high scan rates. About 66.7% retention of specific capacitance is observed at the rapid scan rates of 300 mV s^{-1}. Retention of the large specific capacitance of MCFC-900 is due to the well-defined 3D cubic structure which provides a large area electrode-electrolyte contact facilitating the storage of ionic species.[15, 16] The CV profiles of MCFC (Fig. S13), MCFC-1500 (Fig. S14a) and MCFC-2000 (Fig. S14b) also exhibit characteristic of EDLCs but their specific capacitance value is very low compared to MCFC-900 due to their low specific surface areas. Specific capacitance of MCFC is found is ca. 1.9 F g^{-1} at a scan rate 5 mVs^{-1}. We also conducted galvanostatic charge–discharge experiments in order to obtain further information regarding the capacitive properties of MCFC-900. Charge–discharge profiles at different current densities are shown in Fig. 5d. Charge–discharge profiles of MCFC, MCFC-1500 and MCFC-2000 at 1 A g^{-1} is supplied in Fig. S15. The triangular charge–discharge profile confirms the large capacitance of MCFC-900, which is attributed to the EDLC mechanism. A high specific capacitance of ca. 205 F g^{-1} at a current density 1 A g^{-1} was obtained from the charge–discharge profile (Fig. 5d). Importantly, we have also observed a very high retention of specific capacitance of approximately 56.0 % at very high current density 20 Ag^{-1} demonstrating high rate performance of MCFC-900 (Fig. 5e).[35-38] Cyclic stability of electrode materials is also an important feature in the preparation of efficient supercapacitor devices. The cyclic stability of MCFC-900 at a current density 7 Ag^{-1} was therefore assessed revealing no capacity loss after 10,000 cycles. Specific capacitance actually minutely increases during the initial 2500 cycles subsequently remaining constant (Fig. 5f). The initially gradually improving specific capacitance could be due to improvements in ion accessibility of the porous cubic carbon during the cycling process, which leads to an increased storage capacity of electrolyte ions.[39] Furthermore, MCFC-900 exhibits very high specific capacitance greater than other carbon materials like mesoporous fullerene crystals,[40,41] pure graphene,[42] graphene aerogel,[43,44] two-dimensional graphene-based mesoporous carbon sheets,[45] activated carbon,[46,47] conventional mesoporous carbon,[48-50] nitrogen doped carbon,[51,52] boron doped carbon,[53,54] and carbon nanotube (Table S5).[55,56] The excellent capacitive properties of MCFC-900 are attributed to its large surface area and 3D cube morphology which enhances the electrode-electrolyte interface and improves the accumulation of ions within the mesoporous framework.

Electrochemical Impedance Spectroscopy (EIS) provides in-depth information regarding physical parameters such as diffusion kinetics of the electrolytes, electron-transfer resistance, and double-layer charging at the electrode/electrolyte interface.[57,58] The Nyquist plot of MCFC-2000 shows ideal EDLC type capacitor behavior lacking a semicircular trace in the high frequency region (Fig. 6a). A very steep rise with shorter linear gradients indicates the fast ion transport within the MCFC-2000 electrode. The X-axis intercept of the imaginary component of impedance (Z″) provides quantitative data regarding the series resistance which is ca. 5.7 Ω for MCFC-2000. EIS measurement of MCFC-900 exhibits a partly semicircular trace in the high-frequency region with a straight line at low frequencies, which is an indication of pseudocapacitive behaviour of MCFC-900 electrode.

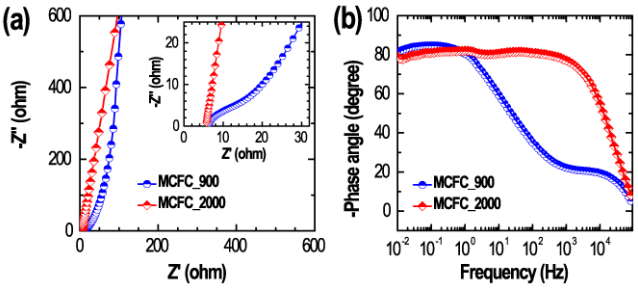

Fig. 6 (a) Nyquist plots of MCFC-900 and MCFC-2000 and (b) Impedance phase angle versus frequency (Bode plot) for MCFC-900 and MCFC-2000.

Pseudocapacitance behavior of MCFC-900 can be attributed to oxygen-containing functional groups whose presence was confirmed by XPS. Series resistance obtained for MCFC-900 ca. 6.4 Ω is slightly larger than for MCFC-2000 (5.7 Ω). Charge transfer resistance obtained from the semicircle trace for MCFC-900 is ca. 8.54 Ω. The dependence of phase angle on the frequency for MCFC-900 and MCFC-2000 is shown in Fig. 6b. The phase angle in the low frequency region for both the samples is close to 80°, which indicates the ideally capacitive nature of the samples.[59] Characteristic frequency for phase angle -45° is 38.3 Hz for MCFC-900 and 14,700 Hz for MCFC-2000. The corresponding time constant obtained for MCFC-900 is 26 ms, which is much lower than that of the commercial active carbon (10-100 s).[60] All the analyses indicate that MCFC-900 and MCFC-2000 are ideal supercapacitor materials. Although, MCFC-2000 exhibits better EIS characteristic than MCFC-900, the capacitance value for MCFC-900 is significantly greater than MCFC-2000. This can be accounted for by the very high surface area and large pore volume of MCFC-900 over MCFC-2000. High porosity and large surface area leads to an increased flux of ions in MCFC-900, which leads in turn to an improved EDLC performance over MCFC-2000.

Conclusions

In summary, we have successfully converted mesoporous crystalline fullerene C_{70} cubes (MCFC) into mesoporous carbon cubes with amorphous (MCFC-900) and graphitic carbon structure (MCFC-2000) by high temperature heat treatments at 900 and 2000 °C. After carbonization, the original cubic morphology of MCFC is retained in MCFC-900, while it is partially destroyed in MCFC-2000. The BET surface area of graphitized MCFC-2000 (ca. 70 m^2g^{-1}) is lower than that of amorphous MCFC-900 (ca. 388 m^2g^{-1}) because of the denser graphitic structure of the MCFC_2000. Due to high surface area and well developed mesoporous structure, MCFC-900 shows excellent capacitive performance exhibiting very high specific capacitance of 286 F g^{-1} at a scan rate 5 mV s^{-1} and 205 F g^{-1} at

current density 1 A g^{-1}. Furthermore, MCFC-900 displays good rate performance and long cyclic stability. We believe that this novel mesoporous carbon with cubic shaped morphology is a potential electrode material for high rate performance electrochemical supercapacitors and other energy-related applications.

Acknowledgements

This study was partially funded by JSPS KAKENHI Grant Number JP 16H06518 (Coordination Asymmetry) and CREST JST Grant Number JPMJCR1665.

Reference

1 J. R. Miller and P. Simon, *Science*, 2008, **321**, 651–652.
2 P. Simon and Y. Gogotsi, *Nat. Mater.*, 2008, **7**, 845–854.
3 G. Wang, L. Zhang and J. Zhang, *Chem. Soc. Rev.*, 2012, **41**, 797–828.
4 Y. Wang and Y. Xia, *Adv. Mater.,* 2013, **25**, 5336–5342.
5 D. Sheberla, J. C. Bachman, J. S. Elias, C.-J. Sun, Y. S.-Horn and M. Dincă, *Nat. Mater*., 2017, **16**, 220–224.
6 R. R. Salunkhe, J. Lin, V. Malgras, S. X. Dou, J. H. Kim and Y. Yamauchi, *Nano Energy*, 2015, 11, 211–218.
7 S.-M. Chen, R. Ramachandran, V. Mani and R. Saraswathi, *Int. J. Electrochem. Sci.*, 2014, **9**, 4072-4085.
8 C. Liang, Z. Li and S. Dai, *Angew. Chem. Int. Ed*. 2008, **47**, 3696–3717.
9 J. Lee, S. Yoon, T. Hyeon, S. M. Oh and K. B. Kim, *Chem. Commun.*, 1999, 2177–2178.
10 C. Liang and S. Dai, *J. Am. Chem. Soc.*, 2006, **128**, 5316–5317.
11 V. Malgras, Q. Ji, Y. Kamachi, T. Mori, F.-K. Shieh, K. C.-W. Wu, K. Ariga and Y. Yamauchi, *Bull. Chem. Soc. Jpn*. 2015, **88**, 1171–1200.
12 S.A. Han, J. Lee, K. Shim, J. Lin, M. Shahabuddin, J.-W. Lee, S.-W. Kim, M.-S. Park, J. H. Kim, *Bull. Chem. Soc. Jpn*. 2018, **91**, 1474–1480.
13 J. Kim, C. Young, J. Lee, Y.-U. Heo, M.-S. Park, M. S. A. Hossain, Y. Yamauchi, J. H. Kim, *J. Mater. Chem. A*, 2017, **5**, 15065-15072.
14 J. Kim, C. Young, J. Lee, M.-S. Park, M. Shahabuddin, Y. Yamauchi, J. H. Kim, *Chem. Commun.* 2016, **52**, 13016–13019.
15 Z. Yu, L. Tetard, L. Zhai and J. Thomas, *Energy Environ. Sci*., 2015, **8**, 702–730.
16 M. Zhi, C. Xiang, J. Li, M. Li and N. Wu, *Nanoscale*, 2013, **5**, 72–88.
17 L. K. Shrestha, Q. Ji, T. Mori, K. Miyazawa, Y. Yamauchi, J. P. Hill, and K. Ariga, *Chem. Asian J*. 2013, **8**, 1662–1679.
18 K. Miyazawa, *Sci. Technol. Adv. Mater*., 2015, **16**, 013502.
19 P. Bairi, K. Minami, J. P. Hill, W. Nakanishi, L. K. Shrestha, C. Liu, K. Harano, E. Nakamura and K. Ariga, *ACS Nano*, 2016, **10**, 8796–8802.
20 P. Bairi, K. Minami, W. Nakanishi, J. P. Hill, K. Ariga and L. K. Shrestha, *ACS Nano*, 2016, **10**, 6631–6637.
21 L. K. Shrestha, R. G. Shrestha, Y. Yamauchi, J. P. Hill, T. Nishimura, K. Miyazawa, T. Kawai, S. Okada, K. Wakabayashi, and K. Ariga, *Angew. Chem. Int. Ed*. 2015, **54**, 951–955.
22 P. Bairi, R. G. Shrestha, J. P. Hill, T. Nishimura, K. Ariga and L. K. Shrestha, *J. Mater. Chem. A*, 2016, **4**, 13899–13906.
23 L. K. Shrestha, R. G. Shrestha, J. P. Hill, T. Tsuruoka, Q. Ji, T. Nishimura and K. Ariga, *Langmuir*, 2016, **32**, 12511−12519.
24 P. Bairi, T. Tsuruoka, S. Acharya, Q. Ji, J. P. Hill, K. Ariga, Y. Yamauchi, L. K. Shrestha, *Mater. Horiz.,* 2018, **5**, 285–290.
25 M. Premila, C. S. Sundar, P. C. Sahu, A. Bharathi, Y. Hariharan, D. V. S. Muthu and A. K. Sood, *Solid State Commun.,* 1997, **104**, 237−242.
26 V. Schettino, M. Pagliai and G. Cardini, *J. Phys. Chem. A*, 2002, **106**, 1815–1823.
27 M. A. Pimenta, G. Dresselhaus, M. S. Dresselhaus, L. G. Cancado, A. Jorioa and R. Saito, *Phys. Chem. Chem. Phys*., 2007, **9**, 1276–1291.
28 1. Z. Tan, K. Ni, G. Chen, W. Zeng, Z. Tao, M. Ikram, Q. Zhang, H. Wang, L. Sun, X. Zhu, X. Wu, H. Ji, R. S. Ruoff and Y. Zhu, *Adv. Mater.*, 2017, **29**, 1603414.
29 2. S. Zheng, H. Ju and X. Lu , *Adv. Energy Mater.*, 2015, **5**, 1500871
30 F. Béguin, V. Presser, A. Balducci and E. Frackowiak, *Adv. Mater.* 2014, **26**, 2219–2251.
31 M. Sevilla and R. Mokaya, *Energy Environ. Sci*., 2014, **7**, 1250–1280.
32 M. Pumera, *Electrochem. Commun.*, 2013, **36**, 14–18.
33 A. Ambrosi, C. K. Chua, A. Bonanni and M. Pumera, *Chem. Rev.*, 2014, **114**, 7150–7188.
34 R. Liu, L. Wan, S. Liu, L. Pan, D. Wu and D. Zhao, *Adv. Funct. Mater*., 2015, **25**, 526–533.
35 X. Wang, C. Yan, A. Sumboja, J. Yan and P. S. Lee, *Adv. Energy Mater*. 2014, **4**, 1301240.
36 L. Ren, G. Zhang, Z. Yan, L. Kang, H. Xu, F. Shi, Z. Lei and Z.-H. Liu, *ACS Appl. Mater. Interfaces*, 2015, **7**, 28294−28302.
37 H. Jiang, J. Ma and C. Li, *Chem. Commun*., 2012, **48**, 4465–4467.
38 (d) Q. Wang, J. Yan, Y. Wang, T. Wei, M. Zhang, X. Jing and Z. Fan, *Carbon*, 2014, **67**, 119–127.
39 Z.-S. Wu, Y. Sun, Y.-Z. Tan, S. Yang, X. Feng and K. Mullen, *J. Am. Chem. Soc*., 2012, **134**, 19532−19535.
40 M. R. Benzigar, S. Joseph, A. V. Baskar, D. -H. Park, G. Chandra, S. Umapathy, S. N. Talapaneni and A. Vinu, *Adv. Funct. Mater.*, 2018, **28**, 1803701.
41 M. R. Benzigar, S. Joseph, H. Ilbeygi, D.-H. Park, S. Sarkar, G. Chandra, S. Umapathy, S. Srinivasan, S. N. Talapaneni and A. Vinu, Angew. Chem., 2018, 130, 578–582.
42 M. D. Stoller, S. Park, Y. Zhu, J. An and R. S. Ruoff, *Nano letter*, 2008, **8**, 3498–3502.
43 Y. Xu, K. Sheng, C. Li and G. Shi, *ACS Nano*, 2010, **4**, 4324–4330.
44 X. Zhang, Z. Sui, B. Xu, S. Yue, Y. Luo, W. Zhan and B. Liu, *J. Mater. Chem*., 2011, **21**, 6494–6497
45 P. Zhang, Z.-A. Qia, Z. Zhang, S. Wana and S. Dai, *J. Mater. Chem. A,* 2014*,* **2***,* 12262–12269.
46 D. Qu and H. Shi, *J. Power Sources*, 1998, **74**, 99–107.
47 M.-H. Kim, K.-Bum Kim, S.-M. Park and K. C. Roh, *Sci. Rep*. 2016, **6**, 21182.
48 H. Lu, W. Dai, M. Zheng, N. Li, G. Ji and J. Cao, *J. Power Sources*, 2012, **209**, 243–250.
49 S.R.S. Prabaharan, R. Vimala and Z. Zainal, *J. Power Sources*, 2006, **161**, 730–736.
50 D. Tang, S. Hu, F. Dai, R. Yi, M. L. Gordin, S. Chen, J. Song and D. Wang, *ACS Appl. Mater. Interfaces*, 2016, **8**, 6779−6783.
51 L.-F. Chen, X.-D. Zhang, H.-W. Liang, M. Kong, Q.-F. Guan, P. Chen, Z.-Y. Wu and S.-H. Yu, *ACS Nano*, 2012, **6**, 7092–7102.
52 W.-h. Lee and J. H. Moon, *ACS Appl. Mater. Interfaces*, 2014, **6**, 13968−13976.
53 D.-W. Wang, F. Li, Z.-G. Chen, G. Q. Lu and H.-M. Cheng, *Chem. Mater*. 2008, **20**, 7195–7200.
54 Z.-S. Wu, A. Winter, L. Chen, Y. Sun, A. Turchanin, X. Feng and K. Müllen, *Adv. Mater*., 2012, **24**, 5130–5135.
55 K. H. An, W. S. Kim, Y. S. Park, Y. C. Choi, S. M. Lee, D. C. Chung, D. J. Bae, S. C. Lim and Y. H. Lee, *Adv. Mater*., 2001, **13**, 497–500.
56 C. Niu, E. K. Sichel, R. Hoch, D. Moy and H. Tennent, *Appl. Phys. Lett*., 2016, **70**, 1480–1482.
57 D. D. Macdonald, *Electrochim. Acta* 2006, **51**, 1376−1388.

58 M. Arunkumar and A. Paul, **ACS Omega** 2017, **2**, 8039−8050.
59 M. F. El-Kady, V. Strong, S. Dubin and R. B. Kaner, *Science*, 2012, **335**, 1326−1330.
60 L. Wei, M. Sevilla, A. B. Fuertes, R. Mokaya and G. Yushin, *Adv. Energy Mater.*, 2011, **1**, 356−361.

Table of content

Mesoporous Carbon Cubes Derived from Fullerene Crystals as a High Rate Performance Electrode Material for Supercapacitors

Partha Bairi,[a] Subrata Maji,[a] Jonathan P. Hill,[a] Jung Ho Kim,[b] Katsuhiko Ariga [a,c] and Lok Kumar Shrestha[a]*

Mesoporous carbon cubes derived from high temperature heat-treatment of mesoporous crystalline fullerene C_{70} cubes showed excellent electrochemical supercapacitive performance.